agronomy

MDPI

Article

Estimating Leaf Water Content through Low-Cost LiDAR

Akira Hama *, Yutaro Matsumoto and Nobuhiro Matsuoka

Graduate School of Horticulture, Chiba University, 648, Matsudo, Matsudo-shi 271-8510, Japan; a4k4i8r8a@yahoo.co.jp (Y.M.); matsuoka@faculty.chiba-u.jp (N.M.)
* Correspondence: a.hama@chiba-u.jp

Abstract: In recent years, rapid development has been achieved in technologies and sensors related to autonomous driving and assistive technologies. In this study, low-cost light detection and ranging (LiDAR) was used to estimate leaf water content (LWC) by measuring LiDAR reflectance instead of morphological measurement (e.g., plant size), which is the conventional method. Experimental results suggest that reflection intensity can be corrected using the body temperature of LiDAR, when using reflection intensity observed by LiDAR. Comparisons of corrected LiDAR observation data and changes in reflectance attributed to leaf drying suggest that the reflectance increases with leaf drying in the 905 nm band observed with a hyperspectral camera. The LWC is estimated with an R^2 of 0.950, RMSE of 6.78%, and MAPE of 18.6% using LiDAR reflectance. Although the 905 nm wavelength used by LiDAR is not the main water absorption band, the reflectance is closely related to the leaf structure; therefore, it is believed that the reflectance changes with structural changes accompanying drying, which allows for the indirect estimation of LWC. This can help utilize the reflectance of the 905 nm single-wavelength LiDAR, which, to the best of our knowledge has not been used in plant observations for estimating LWC.

Keywords: LiDAR; sensing; reflectance; water stress; leaf water content

Citation: Hama, A.; Matsumoto, Y.; Matsuoka, N. Estimating Leaf Water Content through Low-Cost LiDAR. *Agronomy* **2022**, *12*, 1183. https://doi.org/10.3390/agronomy12051183

Academic Editors: José Ramón Rodríguez-Pérez and Shawn C. Kefauver

Received: 31 March 2022
Accepted: 12 May 2022
Published: 14 May 2022

1. Introduction

Recent years have witnessed rapid developments in technologies and sensors related to autonomous driving and driving support [1]. Among these developments, light detection and ranging (LiDAR), which measures the distance from the time-of-flight of light to an object, has been widely used for recognizing the surrounding environment in the context of autonomous driving; daily advances are being reported for the associated technologies and sensors [2]. Low-cost sensors not only broaden the base of LiDAR use but are also advantageous to all fields associated with LiDAR, e.g., agriculture. Sensing technologies that acquire information related to the growth state of crops in a comprehensive and rapid manner have become increasingly important in a social context because they help to minimize labor requirements and labor intensity, and increase refinement in both the research and application aspects of agriculture.

LiDAR was originally developed for airborne laser scanning, and it has been used for forest surveys prior to its use in agriculture. Structures with gaps such as a canopy allow for part of the laser to pass without hitting the plant; this part of the laser is then reflected inside the canopy and on the ground surface. In such cases, multiple reflections (returns) are recorded for each laser pulse; this is called a multireturn [3]. The final return is attributed to the ground; this is useful for acquiring topographical information regarding locations where vegetation has been removed. A point cloud obtained in this manner was used for estimating the height and volume of a single tree [4], estimating the forest growth [5], and classifying tree species [6]. In addition, the return from the ground decreases when the vegetation is densely packed [7], and therefore, this has been used in an attempt to estimate the leaf area index (LAI) [8].

The subsequently developed terrestrial laser scanning has a narrower scope of measurement when compared with its airborne counterpart; however, this type of scanning facilitates the measurement of the subcanopy structure of trees, which could not be covered thus far. Furthermore, the laser beam diameter is smaller, which enables the laser to penetrate the canopy and makes it easier to obtain shape information inside the canopy [9].

The application of LiDAR for agriculture started with fruit trees [10]; it is now being applied to target smaller crops and to protected horticulture [11]. Application examples include the estimation of plant height/community volume [12], leaf angle [13], LAI [11], vegetation coverage/above-ground biomass [14], and yield [15]. Sofonia et al. (2019) [16] suggest that LiDAR not only has the same level of accuracy as the structure from motion (SfM)—a photogrammetric technique—for grass height measurement, but it can also separate the ground surface and crops throughout the growing season, whereas the SfM cannot restore the ground surface shape as crop growth progresses. The height of the ground surface serves as a reference plane for measuring the height of grass, and therefore, obtaining information on the ground surface at each measurement leads to a reduction in the measurement error, and it can be used for estimating biomass.

Based on the aforementioned studies, LiDAR is primarily used for the measurement of the size and shape of plants. Meanwhile, the reflection intensity obtained by LiDAR has thus far only been used to improve the visibility by color-coding the point cloud based on the difference in reflection depending on the object, such as the ground or an inhabited area [17]. The reflection intensity reflects the spectral reflection characteristics at that wavelength, and therefore, LiDAR can overcome the weaknesses of remote sensing techniques using conventional passive sensors that are influenced by soil or lower vegetation. This advantage is attributed to the LiDAR characteristics of using an active sensor and simultaneously obtaining three-dimensional (3D) information. Thus, a wide-ranging utilization of this technology is expected.

The wavelength near the absorption band of that substance is used when estimating the content of a given substance in remote sensing that utilizes spectral reflection characteristics. For example, chlorophyll strongly absorbs wavelengths around 400–700 nm, and water absorbs wavelengths around 1300–2300 nm. Furthermore, there have been studies that focus on this spectral reflection characteristic in LiDAR, with one study estimating the in-leaf chlorophyll content using a 532 nm single-wavelength LiDAR [18]. Du et al. (2016) [19] obtained reflection intensities of 538–910 nm using hyperspectral LiDAR with continuously variable wavelengths and estimated the in-leaf nitrogen content by combining multiple wavelengths. For estimating the leaf water content (LWC), Junttila et al. (2018) [14] used three types of single-wavelength LiDAR (690, 905, and 1550 nm) and two-wavelength reflection intensity ratios to estimate the LWC. Zhu et al. (2015, 2017) [20,21] showed that LWC can be estimated using the reflection intensity of 1550 nm single-wavelength LiDAR; this is near the absorption band of water.

Currently, LiDAR using the single wavelength of 905 nm has become mainstream because this wavelength does not interfere with other sensors (e.g., cameras, human eyes); furthermore, solar radiation, which is a source of noise, is weak at this wavelength, and the sensor that detects the reflected light is inexpensive [22]. There have been many research examples that used LiDAR reflection intensity; however, these existing methods cannot be applied to the 905 nm single-wavelength LiDAR because the wavelength is different or because multiple wavelengths are used.

It is possible to use the changes in reflectance that accompany leaf drying when using the spectral reflectance characteristics of leaves near 905 nm. Drying leaves induce the highest increase in reflectance in the range 350–2500 nm [23]. The increase in reflectance with drying, even at wavelengths below 1300 nm where water absorption is low, can be attributed to the decrease in chlorophyll and changes in the internal structure of the leaf. As drying progresses, the stress results in the decomposition of chloroplasts and the occurrence of plasmolysis due to a decrease in turgor pressure, resulting in an air invasion between the cell wall and cell membrane; this changes the number of refractions and the index of

refraction of light that passes through the leaves. Therefore, the proportion of light returned in the incident direction increases, which further increases the reflectance [24]. This reaction is extremely wavelength-dependent, and therefore, it is useful for estimating water content in regions other than the water absorption band.

Previous studies applied the knowledge of remote sensing using the spectral reflection characteristics from plants, and they clarified that the growth state of plants could be estimated using the wavelength corresponding to the absorption bands of chlorophyll or water; this confirms the usability of the reflection intensity in LiDAR. Moreover, there is the possibility that changes in water content in the wavelength band below 1300 nm can be indirectly detected from changes in cell structure associated with drying. Most single-wavelength LiDAR uses 905 nm, and therefore, the ability to estimate water content using this wavelength provides new possibilities by providing not only 3D data but also reflection intensity to LiDAR applications. Thus, in this study, a 905 nm single-wavelength LiDAR was used to observe changes in the reflection intensity accompanying leaf drying and estimate LWC.

2. Materials and Methods

This study was conducted in a laboratory based on the following process to achieve the stated objectives (Figure 1). During the experiment, the blinds in the laboratory were closed to prevent direct sunlight from entering.

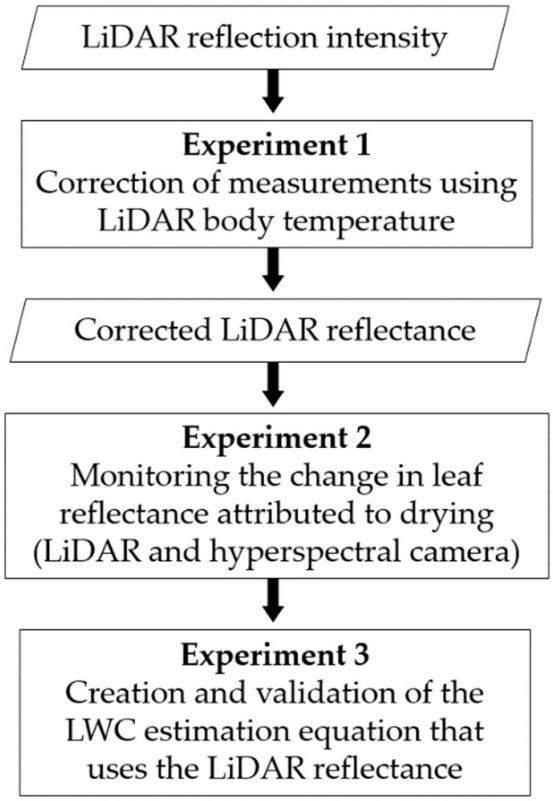

Figure 1. Flowchart of the experiment for LWC estimation.

2.1. Observation Equipment, and Leaf Samples

In this study, the leaves of sweet potatoes (cultivar: Beni-haruka, Beni-azuma) were used as samples for measuring the LWC. The leaves were attached to a plastic cardboard panel with a MicaSense 51% standard reflection panel placed in the center (Photo 1). A Mid-70 (Livox) was the LiDAR used for the observation. A near-infrared laser with a wavelength of 905 nm was used. This LiDAR is a model developed for autonomous driving, and the main unit price was USD 1099 (as of May 2022), which was lower than that of the conventional LiDAR [14,20,21] (Table 1). The conventional LiDAR is 7.9–36.3 times more

expensive than Mid-70. The Livox LiDAR adopts a characteristic laser scanning pattern called the non-repetitive scanning method; this pattern can improve the coverage within the viewing angle compared with that of the conventional horizontal linear scanning method. The sensor does not have a built-in GNSS or IMU. Table 2 summarizes the main specifications. Images were captured using a hyperspectral camera (NH-7, Eba Japan Co., Ltd. Tokyo, Japan) and observations were obtained using LiDAR simultaneously; changes in the spectral reflection characteristics of the leaves attributed to drying were observed. With the NH-7, the measurements could be conducted in the shooting wavelength band of 350–1100 nm with a wavelength resolution of 5 nm. A 500 W halogen lamp was used as the light source during shooting. As a general rule, the error of reflection intensity in LiDAR will be large if the shooting distance is too close to the object (according to the specifications, the error will be large if the distance is less than 2 m). Meanwhile, the footprint becomes larger with a greater distance, and this is affected by reflections from objects other than the leaves or standard reflection panel; therefore, the distance was set to 5 m in this study.

Table 1. A price list of conventional LiDAR and Livox Mid-70 (as of May 2022).

Sensor	Price (USD)	References
Leica HDS6100	18,000	
FARO Focus3D S120	8700	Junttila et al. (2018) [14]
FARO Focus3D X330	30,000	
RIEGL VZ-400	39,900	Zhu et al. (2015, 2017) [20,21]
Livox Mid-70	1099	This study

Table 2. The main specifications of Mid-70 (Livox).

Item	Specification
Laser Wavelength	905 nm
Point Rate	100,000 points/s (first or strongest return) 200,000 points/s (dual return)
Detection Range	0.05–260 m
Range Precision	≤2 cm @ 20 m
Angular Precision	<0.1°
FOV	70.4° (Circular)
Beam Divergence	0.28° (Vertical) × 0.03° (Horizontal)
Weight	580 g
Dimensions	97 × 64 × 62.7 mm

2.2. Correction of Measurements Using LiDAR Body Temperature (Experiment 1)

The intensity of the laser received by the LiDAR is described by the radar equation. According to Wagner (2010) [25], when the surface of the object reflected by the laser is a Lambert surface, the received output, *Pr* (unit: W), is expressed as

$$P_r = \frac{P_t D_r^2 \rho_\lambda cos\alpha}{4R^2} \eta_{atm} \eta_{sys}, \quad (1)$$

where P_t, D_r, ρ_λ, α, R, η_{atm}, and η_{sys} represent the transmission output (W), sensor receiving aperture (m), reflectance at wavelength λ, incident angle, distance (m), atmospheric permeability coefficient, and system transmission efficiency, respectively. Among these variables, the transmission output and sensor receiving aperture, reflectance at wavelength λ, and incident angle and distance, depend on the device, object, and shooting conditions, respectively. Other parameters need to be corrected to obtain the reflectance of the object from the received output accurately. First, the transmission output and sensor receiving aperture are considered as sensor-specific constants. The atmospheric permeability coefficient depends on the atmospheric conditions (e.g., visibility, temperature, humidity, and aerosol concentration); however, this was assumed to be constant in this study. Based on

the aforementioned assumptions, the parameters to be corrected are system transmission efficiency, incident angle, and distance. The system transmission efficiency depends on the internal temperature of the sensor, and this change based on internal (e.g., warm-up after startup) and external factors (ambient temperature and relative humidity) [26]. In this study, a thermocouple was attached to the surface of the LiDAR body; the recorded body temperature was used to correct the measured values.

In LiDAR, the reflection intensity corresponding to P_r is output; however, the LiDAR used in this study records the digital number (DN) obtained by correcting the influence of distance with the reflection intensity. The DN takes an integer from 0 to 255, and if the object does not have specular reflection, then the DN value of 0–150 corresponds to a reflectance of 0–100%. In this study, a DN corrected using the body temperature of LiDAR was used, shown in Equations (2) and (6).

2.3. LWC Estimation Experiment by LiDAR (Experiments 2 and 3)

2.3.1. Experiment 2

The change in reflectance attributed to drying was monitored as follows:

1. Leaves with no holes or symptoms were selected; a total of eight leaves adjusted to 10 cm × 10 cm were attached to the panel so that wrinkles were not present (Figure 2).
2. The panel was installed perpendicular to the LiDAR and the hyperspectral camera (Figure 3).
3. Reflectance was measured over time with LiDAR and a hyperspectral camera from a point 5 m away.

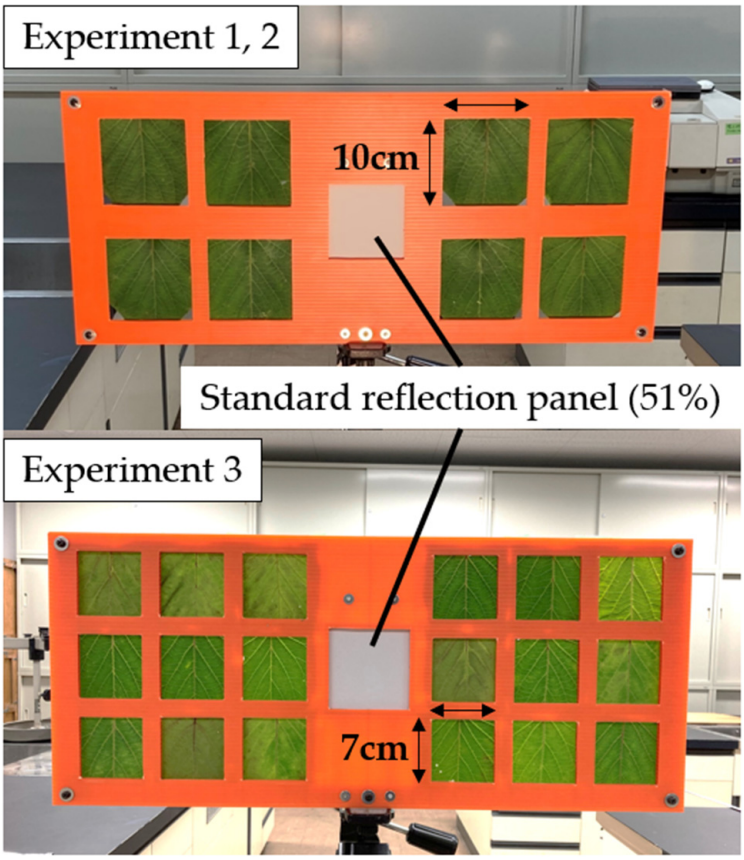

Figure 2. The images of leaf samples.

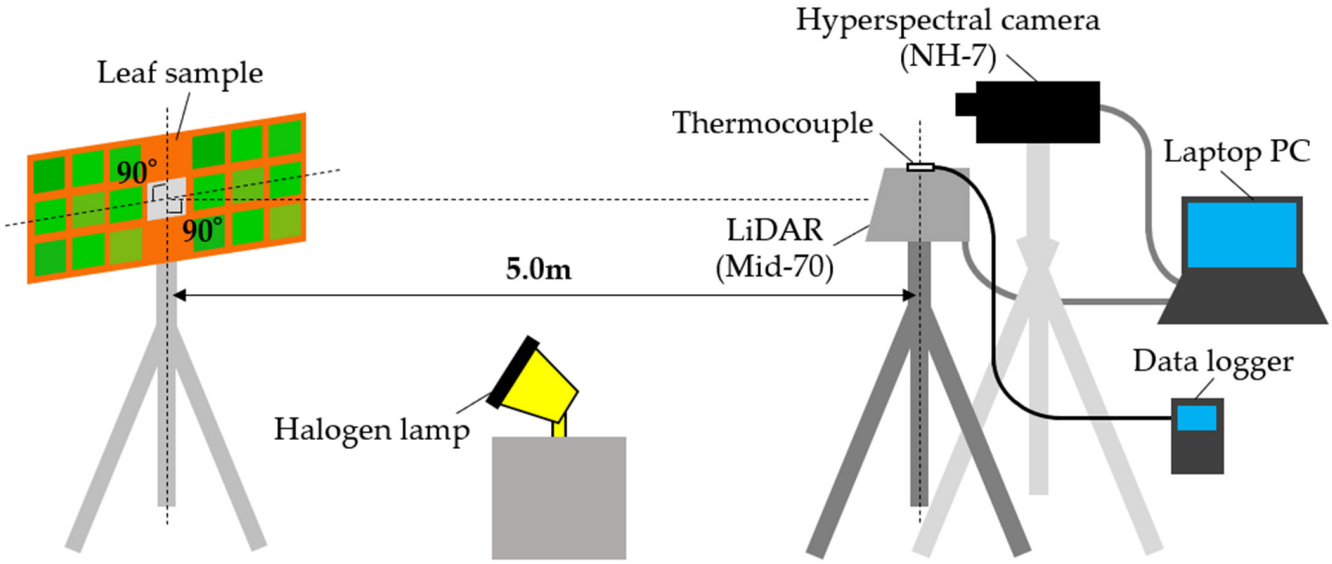

Figure 3. Schematic diagram of the observation.

2.3.2. Experiment 3

The LWC estimation equation that uses the LiDAR reflectance was formulated and verified as follows:

1. Samples with adjusted dryness were prepared by changing the time after leaf collection so that a wide range of water content data could be obtained.
2. A total of 18 leaves adjusted to 7 cm × 7 cm were attached to the panel so that wrinkles were not present (Figure 2).
3. The panel was installed perpendicular to the LiDAR.
4. Reflectance was measured over time with LiDAR from a point 5 m away.
5. After obtaining the reflectance, the fresh biomass of each of the 18 leaves was measured, after which the leaves were dried at 105 °C for 24 h to measure the dry biomass.
6. The same experiment was conducted twice, with the first used for calibrating the LWC estimation equation, and the second for validation.

In Experiment 3, the area of one section of the plastic plate was changed to 7 cm^2 (total number of sections: 18) to increase the number of samples processed per experiment.

2.4. Data and Analysis

2.4.1. Analysis of LiDAR and Hyperspectral Data

Data were acquired for 1 min using the Livox viewer, which is a point cloud data viewing/recording software manufactured by Livox; the collected data were saved in LAS format. Then, the open-source software CloudCompare was used to generate a raster image with a pixel size of 0.5 cm that recorded the average DN in the pixel. Subsequently, after considering the beam divergence angle of LiDAR, the DN of the central 4 cm^2 area, which was unaffected by the surrounding plastic plate, was averaged and used as the DN of the individual leaves. The individual leaf reflectance was obtained by dividing the individual leaf DN by the DN of the standard reflection panel and multiplying it by 51 (%); this is the reflectance of the standard reflection panel and is given as

$$Ref_{leaf} = \frac{DN_{leaf}}{DN_{panel}} \times Ref_{panel}, \quad (2)$$

where Ref_{leaf}, DN_{leaf}, DN_{panel}, and Ref_{panel} represent the leaf reflectance, leaf DN, DN of the standard reflection panel, and reflectance of the standard reflection panel of the leaf (51%), respectively.

The estimation equation was evaluated using the coefficient of determination (R^2) as well as the root mean square error (RMSE) and mean absolute percentage error (MAPE). The calculation equation is

$$\mathrm{RMSE} = \sqrt{\frac{1}{n}\sum_{K=1}^{n}(f_i - y_i)^2}, \tag{3}$$

$$\mathrm{MAPE} = \frac{100}{n}\sum_{k=1}^{n}\left|\frac{f_i - y_i}{y_i}\right|, \tag{4}$$

where n, f_i, and y_i represent the number of data, measured value, and model-estimated value, respectively.

2.4.2. Measurement of Leaf Moisture Content

Sweet potato leaves without any holes or disease were selected, and they were attached to the plastic plate with care to ensure there were no wrinkles. After obtaining the DN, the fresh biomass of the leaves was immediately weighed and dried at 105 °C for 24 h to obtain the dry biomass. The LWC of one sweet potato leaf is defined by

$$\mathrm{LWC} = \frac{\left(B_{fresh} - B_{dry}\right)}{B_{fresh}} \times 100, \tag{5}$$

where LWC denotes the leaf water content (%), B_{fresh} denotes the fresh biomass (g), and B_{dry} represents the dry biomass (g).

3. Results

3.1. Correction Using LiDAR Body Temperature

Figure 4a shows changes over time in the DN of the standard reflection panel and the body temperature of the LiDAR after a cold start. Rapid increases were observed in the body temperature of the LiDAR and decreases were observed in the DN with the start-up, with the changes in values being large in the 30 min period after start-up. The room temperature and humidity were 19.5 °C and 43.6%, respectively, at the start of experiments, and 21.3 °C and 39.8%, respectively, at the end of the experiments. As shown in Figure 4b, a strong correlation was observed between the body temperature of LiDAR and the DN of the standard reflection panel. Therefore, the DN of the standard reflection panel from the LiDAR body temperature was estimated using exponentiation as

$$DN_{panel} = 15{,}502\ BT^{-1.555}, \tag{6}$$

where DN_{panel} represents the DN of the standard reflection panel, and BT represents the body temperature of the LiDAR.

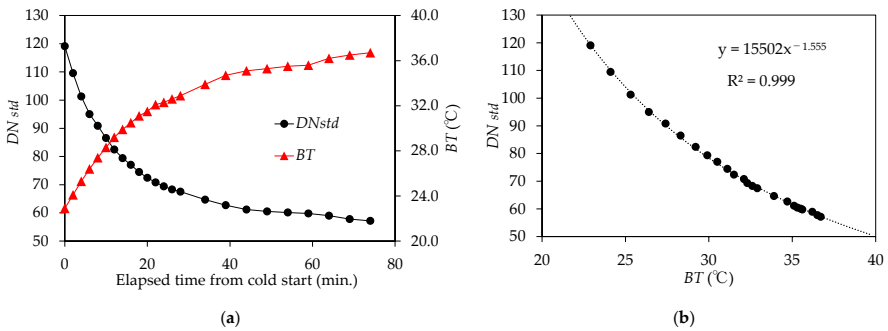

(**a**) (**b**)

Figure 4. Changes over time in the DN of the standard reflection panel (DN_{std}) related to the body temperature of the LiDAR (BT). (**a**) Changes over time in the DN_{std} and the BT after a cold start; (**b**) Correlation between the DN_{std} and the BT. The dashed line denotes the regression line.

3.2. Changes in Reflectance Caused by Leaf Drying

Figure 5 shows the changes in the reflection spectra of the individual sweet potato leaves with drying, as observed by the hyperspectral camera in leaves with the largest change in the LWC in Experiment 2. Reflectance increased in almost all wavelength bands, including 905 nm, from 40 min after the start of experiments to 37 h, after naturally drying in the room. The LWC before the start of experiments was 85.6%, and this decreased to 6.9% at 49 h after the end of the experiments.

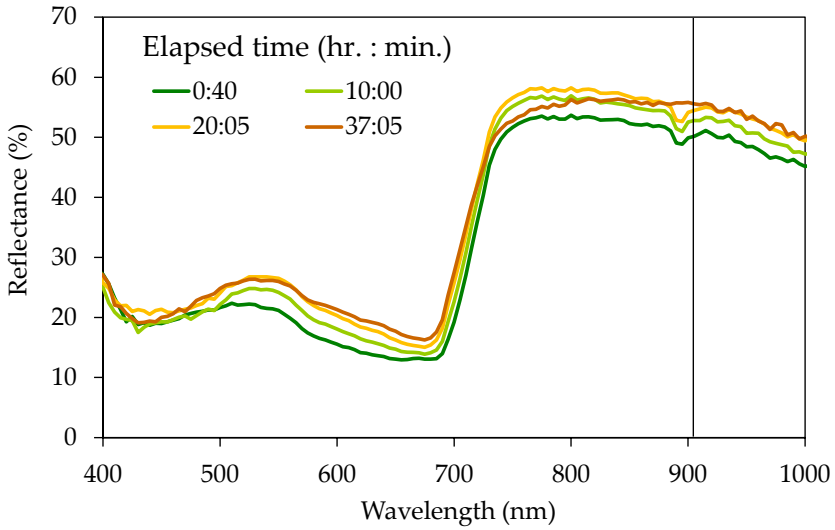

Figure 5. Changes in the reflection spectra of the sweet potato leaves with drying, as observed by the hyperspectral camera. The solid line denotes the LiDAR wavelength 905 nm.

Figure 6a shows the correlation between the reflectance and LWC of the individual sweet potato leaves observed with the LiDAR in Experiments 2 and 3. The reflectance observed with the LiDAR increased with leaf drying, which was also the case with the hyperspectral camera (Figures 5 and 6b). Furthermore, the reflectance of LiDAR and LWC show the same tendencies even when the observation dates are different. The LWC estimation equation using the reflectance of LiDAR is given as

$$\mathrm{LWC} = -0.0451\ Ref_{leaf}{}^2 + 2.37 Ref_{leaf} + 65.6. \quad (7)$$

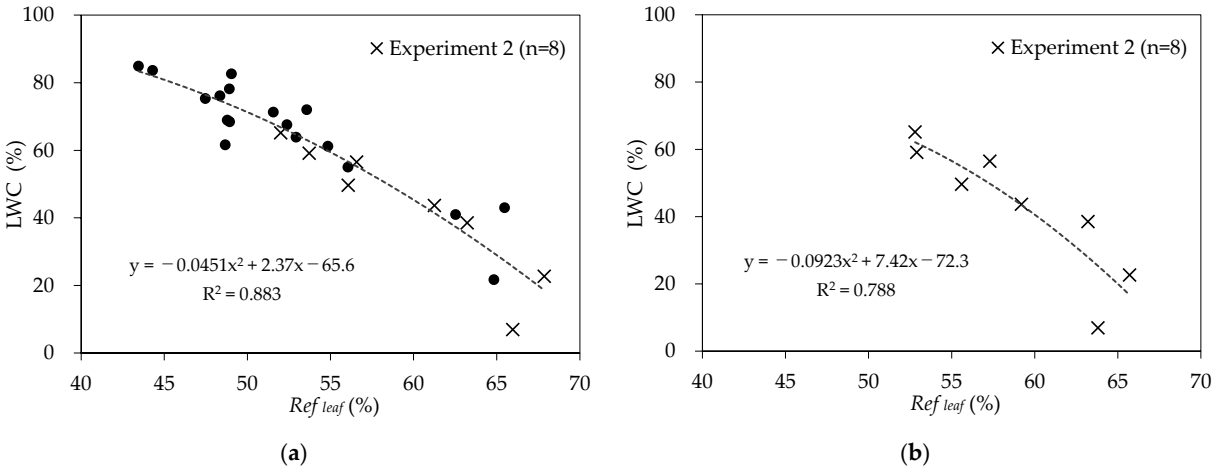

Figure 6. Correlation between the reflectance (*Ref leaf*) and leaf water content (LWC) of the individual sweet potato leaves. (**a**) Result of the LiDAR observation; (**b**) result of the hyperspectral camera observation (905 nm). The dashed line denotes the regression line.

Figure 7 shows the results of verifying the LWC estimation value obtained using Equation (7). The LWC could be estimated with an R^2 of 0.950, RMSE of 6.78%, and MAPE of 18.6%.

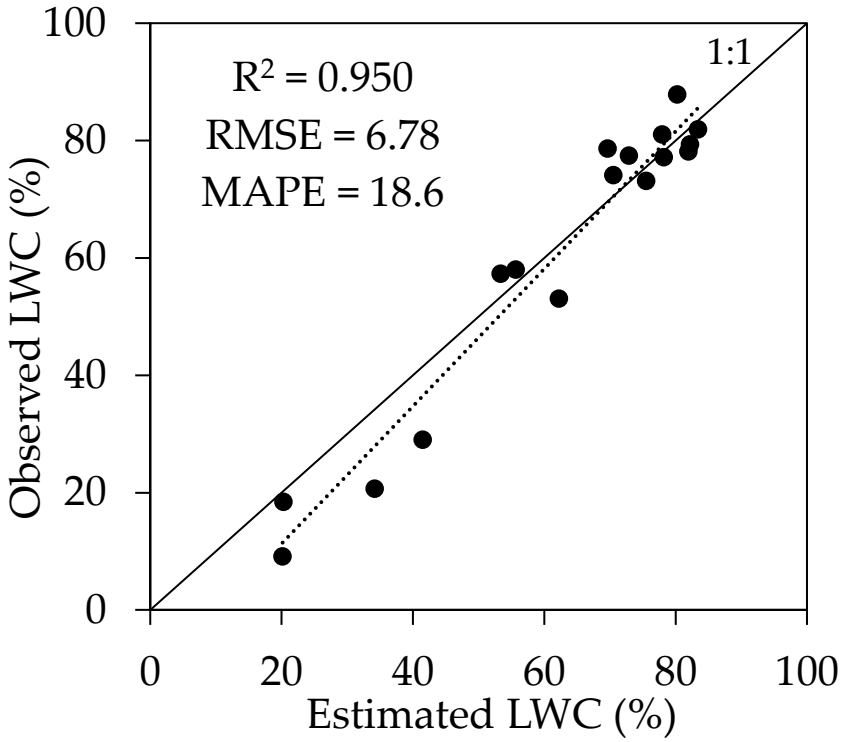

Figure 7. Comparison between estimated and observed leaf water content (LWC). The solid line denotes 1:1 and the dashed line denotes the regression line.

4. Discussion

The body temperature of LiDAR is a useful parameter for correcting the system transmission efficiency; furthermore, LiDAR reflection intensity can be corrected and converted to reflectance without using a standard reflection panel by measuring the body temperature. A standard reflection panel is expensive and needs to be imprinted at the same time as the object, and therefore, it is a constraining factor for the practicality of observations. However, the reflectance of an object can be obtained without using a standard reflection panel when using the body temperature of the LiDAR. Although angle correction is a future task, the 3D mapping of reflectance could be conducted while moving within a field if angle correction is possible. Obtaining reflectance with a passive sensor such as a camera requires the use of a standard reflection panel or simultaneously measuring the incident light and converting it to reflectance; however, it is expected that the use of LiDAR, though limiting applications to specific wavelengths, will allow for an easier acquisition of reflectance values.

Most reflectance in leaves increased in the range from 350 nm to 2500 nm [23]; changes in the reflection spectra accompanying the drying of individual sweet potato leaves obtained with a hyperspectral camera were in agreement with these results. Although the wavelength of 905 nm used by LiDAR is not within the main water absorption band, reflectance is closely related to the leaf structure, and therefore, it is believed that changes in structure alongside drying (invasion of air caused by plasmolysis) resulted in changes to reflectance, which created an indirect correlation with LWC. Thus, utilizing this phenomenon can enable the use of the reflectance of the 905 nm single-wavelength LiDAR, which has not been used in plant observations to date to the best of our knowledge, for estimating LWC.

Water stress is a factor that influences crop productivity, and therefore, understanding LWC is an important element in production management [27]. Thus, comprehensively acquiring the LWC in addition to morphological information can allow for its utilization in stress detection, irrigation timing, and yield prediction applications [28]. Furthermore, 905 nm is the mainstream wavelength used by LiDAR for sensors, and thus, the use of this wavelength provides new possibilities for many LiDAR applications. Furthermore, the leaf structure correlates with the photosynthetic capacity and nitrogen content [29]; the LiDAR reflection intensity may be applicable not only to LWC estimation but also to these estimations.

However, structural changes that accompany drying vary by species, and it has been reported that drying may result in reflectance decreasing further [23]. This can be attributed to the cell wall damage associated with drought [30]. In fact, our sweet potato leaf observations confirmed that reflectance decreased after initially increasing in the 720–880 nm range as drying progressed (Figure 5). A regression equation for the 905 nm wavelength was obtained because the aforementioned effect was not present in this range; however, care should be taken with other plants as the same changes may not occur there.

Finally, there is the possibility that favorable results were obtained because experiments were conducted in a room where sunlight was not directly incident on the plant leaves. A 905 nm wavelength corresponds to a local minimum in the solar spectrum at the Earth's surface caused by absorption by water vapor in the upper atmosphere [22]. However, strong background light (e.g., when direct sunlight is present) becomes a noise in long-range LiDAR observation [31]. It is expected that the same observations can be achieved outdoors at night, during cloudy weather, or with close-range observation; however, further verification will be required for such observations in the daytime, particularly under conditions where direct sunlight is present.

5. Conclusions

Low-cost LiDAR was used to perform LWC estimation using the reflectance of LiDAR instead of measuring the shape of plants.

The results of Experiment 1 show that measuring the body temperature of the LiDAR allowed for LiDAR reflection intensity correction and its conversion to reflectance. This eliminated the constraints associated with standard reflection panel use, and therefore, LiDAR reflectance use became easier.

In Experiments 2 and 3, the corrected LiDAR observation data were compared with changes in reflectance that accompanied changes in the LWC; the results indicate that the reflectance at 905 nm, which is used in LiDAR, and the reflectance measured with LiDAR showed a similar tendency. The same relationship between reflectance and LWC measured with LiDAR was observed regardless of the observation day. The results of estimating LWC using the reflectance of LiDAR show that the LWC could be estimated with an R^2 of 0.950, RMSE of 6.78%, and MAPE of 18.6%.

The wavelength of 905 nm used by LiDAR is not the main water absorption band; however, the reflectance was closely related to the leaf structure, and therefore, it was believed that structural changes accompanying drying resulted in changes in reflectance, which allows for an indirect estimation of the LWC. Furthermore, it was suggested that utilizing this phenomenon can enable the use of the reflectance of the 905 nm single-wavelength LiDAR, which has not been used in plant observations to date to the best of our knowledge, for estimating the LWC. These results show that physiological parameters and plant morphology information could be simultaneously observed with LiDAR applications in plant measurement.

Author Contributions: Conceptualization, A.H. and Y.M.; methodology, A.H. and Y.M.; validation, Y.M.; formal analysis, A.H. and Y.M.; investigation, A.H. and Y.M.; resources, A.H., Y.M. and N.M.; data curation, A.H. and Y.M.; writing—original draft preparation, A.H.; writing—review and editing, N.M.; visualization, A.H. and Y.M.; supervision, N.M.; project administration, N.M.; funding acquisition, A.H. All authors have read and agreed to the published version of the manuscript.

Funding: This work was supported by JSPS KAKENHI (Grant Number 19J00437, 20H01388) and was conducted as a joint research program of CEReS, Chiba University (2021).

Data Availability Statement: Not applicable.

Acknowledgments: We would like to express our sincere thanks to all members of the laboratory of bio-environmental meteorology, Chiba university.

Conflicts of Interest: The authors declare no conflict of interest.

References

1. Claussmann, L.; Revilloud, M.; Gruyer, D.; Glaser, S. A review of motion planning for highway autonomous driving. *IEEE Trans. Intell. Transp. Syst.* **2019**, *21*, 1826–1848. [CrossRef]
2. Li, Y.; Ibanez-Guzman, J. Lidar for autonomous driving: The principles, challenges, and trends for automotive lidar and perception systems. *IEEE Signal Processing Mag.* **2020**, *37*, 50–61. [CrossRef]
3. Hyyppä, J.; Hyyppä, H.; Yu, X.; Kaartinen, H.; Kukko, A.; Holopainen, M. Forest inventory using small-footprint airborne lidar. In *Topographic Laser Ranging and Scanning*; CRC Press: Boca Raton, FL, USA, 2017; pp. 335–370.
4. Ziegler, M.; Konrad, H.; Hofrichter, J.; Wimmer, A.; Ruppert, G.S.; Schardt, M.; Hyyppae, J.M. Assessment of forest attributes and single-tree segmentation by means of laser scanning. In *Laser Radar Technology and Applications V*; SPIE: Bellingham, WA, USA, 2000; pp. 73–84.
5. Yu, X.; Hyyppä, J.; Kaartinen, H.; Maltamo, M. Automatic detection of harvested trees and determination of forest growth using airborne laser scanning. *Remote Sens. Environ.* **2004**, *90*, 451–462. [CrossRef]
6. Li, J.; Hu, B.; Noland, T. Classification of tree species based on structural features derived from high density LiDAR data. *Agric. For. Meteorol.* **2013**, *171*, 104–114. [CrossRef]
7. Harding, D.; Lefsky, M.; Parker, G.; Blair, J. Laser altimeter canopy height profiles: Methods and validation for closed-canopy, broadleaf forests. *Remote Sens. Environ.* **2001**, *76*, 283–297. [CrossRef]
8. Luo, S.; Wang, C.; Pan, F.; Xi, X.; Li, G.; Nie, S.; Xia, S. Estimation of wetland vegetation height and leaf area index using airborne laser scanning data. *Ecol. Indic.* **2015**, *48*, 550–559. [CrossRef]
9. Hosoi, F. Current Status and Future Prospects of Vegetation Measurements Using Laser Scanners. *J. Remote Sens. Soc. Jpn.* **2021**, *41*, 296–298. [CrossRef]
10. Colaço, A.F.; Molin, J.P.; Rosell-Polo, J.R. Application of light detection and ranging and ultrasonic sensors to high-throughput phenotyping and precision horticulture: Current status and challenges. *Hortic. Res.* **2018**, *5*, 35. [CrossRef]
11. Llop, J.; Gil, E.; Llorens, J.; Miranda-Fuentes, A.; Gallart, M. Testing the suitability of a terrestrial 2D LiDAR scanner for canopy characterization of greenhouse tomato crops. *Sensors* **2016**, *16*, 1435. [CrossRef]
12. Sun, S.; Li, C.; Paterson, A.H.; Jiang, Y.; Xu, R.; Robertson, J.S.; Snider, J.L.; Chee, P.W. In-field high throughput phenotyping and cotton plant growth analysis using LiDAR. *Front. Plant Sci.* **2018**, *9*, 16. [CrossRef]
13. Bailey, B.N.; Mahaffee, W.F. Rapid measurement of the three-dimensional distribution of leaf orientation and the leaf angle probability density function using terrestrial LiDAR scanning. *Remote Sens. Environ.* **2017**, *194*, 63–76. [CrossRef]
14. Junttila, S.; Sugano, J.; Vastaranta, M.; Linnakoski, R.; Kaartinen, H.; Kukko, A.; Holopainen, M.; Hyyppä, H.; Hyyppä, J. Can leaf water content be estimated using multispectral terrestrial laser scanning? A case study with Norway spruce seedlings. *Front. Plant Sci.* **2018**, *9*, 299. [CrossRef] [PubMed]
15. Underwood, J.P.; Hung, C.; Whelan, B.; Sukkarieh, S. Mapping almond orchard canopy volume, flowers, fruit and yield using lidar and vision sensors. *Comput. Electron. Agric.* **2016**, *130*, 83–96. [CrossRef]
16. Sofonia, J.; Shendryk, Y.; Phinn, S.; Roelfsema, C.; Kendoul, F.; Skocaj, D. Monitoring sugarcane growth response to varying nitrogen application rates: A comparison of UAV SLAM LiDAR and photogrammetry. *Int. J. Appl. Earth Obs. Geoinf.* **2019**, *82*, 101878. [CrossRef]
17. Tan, K.; Cheng, X. Specular reflection effects elimination in terrestrial laser scanning intensity data using Phong model. *Remote Sens.* **2017**, *9*, 853. [CrossRef]
18. Eitel, J.U.; Vierling, L.A.; Long, D.S. Simultaneous measurements of plant structure and chlorophyll content in broadleaf saplings with a terrestrial laser scanner. *Remote Sens. Environ.* **2010**, *114*, 2229–2237. [CrossRef]
19. Du, L.; Gong, W.; Shi, S.; Yang, J.; Sun, J.; Zhu, B.; Song, S. Estimation of rice leaf nitrogen contents based on hyperspectral LIDAR. *Int. J. Appl. Earth Obs. Geoinf.* **2016**, *44*, 136–143. [CrossRef]
20. Zhu, X.; Wang, T.; Darvishzadeh, R.; Skidmore, A.K.; Niemann, K.O. 3D leaf water content mapping using terrestrial laser scanner backscatter intensity with radiometric correction. *ISPRS J. Photogramm. Remote Sens.* **2015**, *110*, 14–23. [CrossRef]
21. Zhu, X.; Wang, T.; Skidmore, A.K.; Darvishzadeh, R.; Niemann, K.O.; Liu, J. Canopy leaf water content estimated using terrestrial LiDAR. *Agric. For. Meteorol.* **2017**, *232*, 152–162. [CrossRef]
22. Rablau, C. LIDAR–A new (self-driving) vehicle for introducing optics to broader engineering and non-engineering audiences. In Proceedings of the Education and Training in Optics and Photonics, Quebec, QC, Canada, 21–24 May 2019; pp. 11138–11143.
23. Cao, Z.; Wang, Q.; Zheng, C. Best hyperspectral indices for tracing leaf water status as determined from leaf dehydration experiments. *Ecol. Indic.* **2015**, *54*, 96–107. [CrossRef]

24. Carter, G.A. Primary and secondary effects of water content on the spectral reflectance of leaves. *Am. J. Bot.* **1991**, *78*, 916–924. [CrossRef]
25. Wagner, W. Radiometric calibration of small-footprint full-waveform airborne laser scanner measurements: Basic physical concepts. *ISPRS J. Photogramm. Remote Sens.* **2010**, *65*, 505–513. [CrossRef]
26. Larsson, H.; Chevalier, T.; Gustafsson, F. 3-D Structure and Reflectance Measurements: A System Analysis of Lidar Optech ILRIS-3D. *FOI-R. Sens. Syst. Def. Res. Agency (FOI)* **2007**, *102*, 261–285.
27. Zhang, C.; Kovacs, J.M. The application of small unmanned aerial systems for precision agriculture: A review. *Precis. Agric.* **2012**, *13*, 693–712. [CrossRef]
28. Tahara, M.; Carver, B.F.; Johnson, R.C.; Smith, E.L. Relationship between relative water content during reproductive development and winter wheat grain yield. *Euphytica* **1990**, *49*, 255–262. [CrossRef]
29. Reich, P.; Ellsworth, D.; Walters, M. Leaf structure (specific leaf area) modulates photosynthesis-nitrogen relations: Evidence from within and across species and functional groups. *Funct. Ecol.* **1998**, *12*, 948–958. [CrossRef]
30. Seelig, H.D.; Hoehn, A.; Stodieck, L.; Klaus, D.; Adams Iii, W.; Emery, W. The assessment of leaf water content using leaf reflectance ratios in the visible, near-, and short-wave-infrared. *Int. J. Remote Sens.* **2008**, *29*, 3701–3713. [CrossRef]
31. Villa, F.; Severini, F.; Madonini, F.; Zappa, F. SPADs and sipms arrays for long-range high-speed light detection and ranging (LiDAR). *Sensor* **2021**, *21*, 3839. [CrossRef]